

Article

Multi-Objective Design of a Distributed Ducted Fan System

Jiahao Guo and Zhou Zhou *

School of Aeronautics, Northwestern Polytechnical University, Xi'an 710072, China;
guojiahaoxy@mail.nwpu.edu.cn

* Correspondence: zhouzhou@nwpu.edu.cn

Abstract: The distributed propulsion system applied to the vertical take-off and landing aircraft must maintain the high performance in both hover and cruise flight. The gap of the power unit has an adverse effect on the distributed ducted fan system, especially in cruise flight. Therefore, a new distributed ducted fan system was proposed, which eliminated the power gap in design, and adjusted the contraction and expansion of the wake through the deflectable induced wing arranged behind the ducted fan to ensure the high efficiency of the distributed ducted fan system in different flight phases. Then, a multi-objective design method of the distributed ducted fan system was proposed, and the feasibility of the design method was verified by designing the inlet and outlet of the duct and the induced wing. Design results show that the performance change of the distributed ducted fan system mainly came from the change of the inlet. By increasing the length and height of the inlet, the flow separation was alleviated and the duct thrust was increased in hover flight, but the cruise drag became larger. The increase of the inlet height made the operating point of the blade far away in hover and cruise flight, which increased the difficulty of the multi-objective design. Compared with the distributed ducted fan system composed of the traditional circular ducted fan, the hovering power load was reduced by 3.703%, but the cruise efficiency was increased by 17.372%, and the spanwise space was reduced by 20% in the final design.

Keywords: distributed propulsion system; ducted fan; momentum source method; VTOL; multi-objective design



Citation: Guo, J.; Zhou, Z.

Multi-Objective Design of a
Distributed Ducted Fan System.

Aerospace **2022**, *9*, 165. <https://doi.org/10.3390/aerospace9030165>

Received: 28 February 2022

Accepted: 13 March 2022

Published: 17 March 2022

Publisher's Note: MDPI stays neutral with regard to jurisdictional claims in published maps and institutional affiliations.



Copyright: © 2022 by the authors. Licensee MDPI, Basel, Switzerland. This article is an open access article distributed under the terms and conditions of the Creative Commons Attribution (CC BY) license (<https://creativecommons.org/licenses/by/4.0/>).

1. Introduction

In recent years, the electric vertical take-off and landing (VTOL) aircraft has become a research hotspot in aviation due to its characteristics of low emission, low noise, and convenient take-off and landing, such as Lilium jet of German Lilium Company and XV-24A Lightning Strike aircraft of American Aurora Company (Torrance, CA, USA). Both aircraft adopt the distributed propulsion system.

The distributed propulsion system can use boundary layer ingestion (BLI) [1] and wake-filling [2] to improve the propulsion efficiency, increase lift by increasing dynamic pressure [3], reduce requirements for traditional control surfaces and increase the redundancy of the control system, and reduce noise signatures [4,5], making it a competitive solution in future aviation [6]. Studies have shown that N3-X aircraft with turboelectric distributed propulsion (TeDP) [7] to be capable of achieving a 60% reduction in total energy consumption over current aircraft [8]. Wick studied three integration distributed propulsion concepts: Lower TE (Trailing Edge), Upper TE, and Imbedded configurations by using the computational fluid dynamics (CFD) method based on a modified boundary condition, and the results indicated that the Lower TE configuration was the best performer [9]. Kerho studied the influence of fan thrust angle and fan thrust level of the overwing distributed propulsion system using an actuator disk model [10]. Zhang used the momentum source method (MSM) to study the lift enhancement effect of the distributed ducted fan system on a hybrid wing body UAV [11]. However, the above studies simplify the propulsion system, and do not consider the influence of the airframe on the distributed propulsion system.

Both Lilium jet and XV-24A Lightning Strike aircraft used electric ducted fans as the power of the distributed propulsion system, because the ducted fan can generate thrust and reduce the tip losses of blades [12]. The ducted fan in low Mach number has higher aerodynamic efficiency than the propeller with the same disc load. Stubblefield used the lift line model to design the blade of the ducted fan [13]. Guo established an efficient blade design method for the ducted fan by modifying the blade element momentum design method through CFD results [14]. Yu used the panel method and CFD method to optimize the blade of the ducted fan [15]. Ye simplified the blade by MSM, and optimized the NASA duct by using response surface model and neural network model, respectively [16]. Ji used the MSM to analyze and optimize the duct shape of the ducted fan [17]. However, there is still a lack of complete research on the design of the duct and fans of the distributed ducted fan system, especially the multi-objective design in hover and cruise flight.

In order to better integrate with the wing, the distributed ducted fan system generally adopted a rectangular duct [10,18,19]. Bento used the actuator disk model and the steady and unsteady CFD methods to study the influence of the duct shape on the performance of the ducted fan [20]. Sun studied the propulsion characteristics of the distributed ducted fan system with different duct shapes [21]. Their research both showed that the corner of the square duct is prone to a flow separation, resulting in a reduction in the efficiency of the ducted fan. Wang optimized the inlet of the rectangular duct in the distributed propulsion system based on the panel method in hover flight [22]. However, since the panel method cannot predict the flow separation, the accuracy of the optimized design needs to be further improved.

At present, most of the research on the distributed propulsion system focuses on configuration characteristic analysis, and the related design research of the ducted fan focuses on the independent propulsion system and single objective, while the multi-objective design research of the distributed ducted fan system is less. Therefore, this paper first proposed a new distributed ducted fan system for the VTOL aircraft. By establishing the parameterization method of the inlet and outlet of the rectangular duct, and using the efficient MSM to obtain the performance, a multi-objective design method of the distributed ducted fan system was proposed based on NSGA-II algorithm and Kriging model. Finally, the design method was verified by the design comparison.

2. Numerical Simulation Methods

Numerical simulation methods of the ducted fan were verified by using a 150 ducted fan shown in Figures 1 and 2. The duct of the 150 ducted fan has an inlet length of $l_{in} = 40$ mm, an inlet radius of $R_{in} = 90$ mm, a length of the blade section of $l_h = 100$ mm, a hub radius of $R_h = 30$ mm, a radius of the inner wall of $R = 75$ mm, a maximum radius of the outer wall of $R_{max} = 96$ mm, an outlet length of $l_{out} = 100$ mm, and an outlet expansion angle of $\alpha_e = 3^\circ$. The blade number of the rotor is 10 with a blade tip clearance of 0.5 mm, and the blade number of the stator is 6.

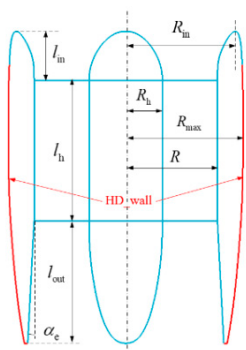


Figure 1. Duct profile of the 150 ducted fan.

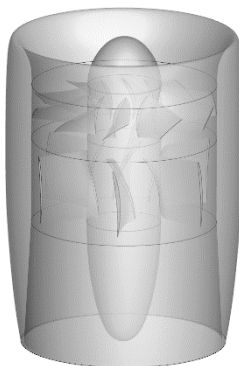


Figure 2. Geometry of the 150 ducted fan.

The performance of the 150 ducted fan was tested under no incoming flow state, as shown in Figure 3. The ATI delta sensor was used to measure the aerodynamic force. The “Eagle tree” was used to measure the rotating speed. The power was supplied by a regulated power supply, and the DC power was converted into AC power by an electric regulator. Each test point was tested stably for 5 s, and the results were obtained by time-averaged processing. Since the “HD_wall” shown in Figure 1 in the test state basically did not generate thrust, it was cancelled during the test to facilitate installation.



Figure 3. Picture of the 150 ducted fan during the test.

The multiple reference frame (MRF) method and MSM [23] were used in the numerical simulation of the ducted fan based on Navier–Stokes (N–S) equations and the $k-\omega$ SST turbulence model. Moreover, the implicit solver formulation, Roe-FDS flux type, and second-order upwind spatial discretization were used. The MRF method adopted the structured grid with 1.04 million background cells and 1.92 million blade cells, as shown in Figure 4. The grid with 1.13 million cells used in the MSM is shown in Figure 5, and the momentum source term was added in the middle part of the duct to be equivalent to the effect of the blade.

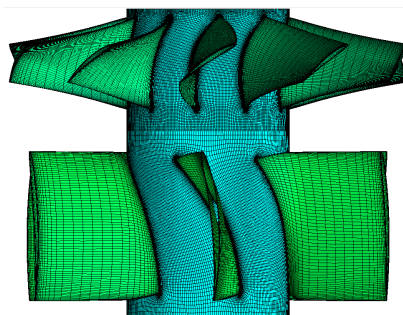


Figure 4. Schematic of the blade grid in the MRF method.

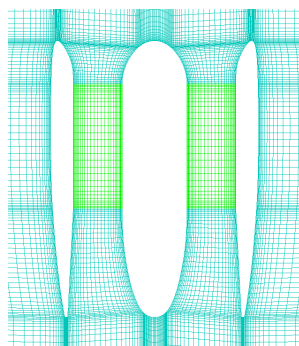


Figure 5. Schematic of the grid in the MSM.

In the MSM, the momentum source term S_m was calculated through Equation (1), where blade thrust T_p is calculated by the corresponding MRF method, and vol is the total volume of the grid to which the momentum source term was added.

$$S_m = T_p / vol \quad (1)$$

The calculation was carried out on a computer using Ryzen 3900X processor of AMD. The result comparison between the two CFD methods and experiment is shown in Figure 6 and Table 1. The errors of the two CFD methods are within 10% near the design point. However, the time consumption of the MSM is only 1/9 of the MRF method. Therefore, the MSM can be used to design the ducted fan, and the MRF method can be used for more accurate characteristic analysis.

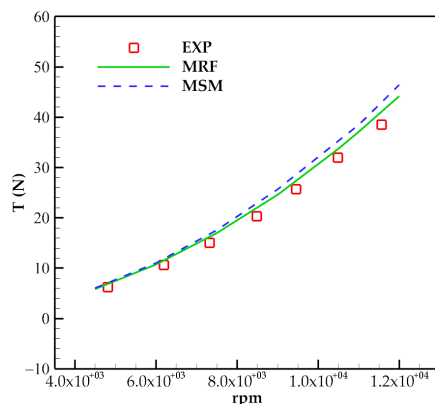


Figure 6. Comparison of the thrust of the ducted fan obtained by different methods.

Table 1. Characteristic comparison of different methods at $\Omega = 10,500$ r/min.

Method	T_p (N)	T_d (N·m)	T (N)	Error	Time (h)
EXP	-	-	32.116	-	-
MRF	15.321	18.404	33.725	5.001%	1.8
MSM	15.321	19.984	35.305	9.930%	0.2

3. Characteristic Analysis of the Distributed Ducted Fan System

3.1. Distributed Ducted Fan System

Traditional circular ducted fans were arranged to form the distributed ducted fan system shown in Figure 7 with a power gap of $d = 5$ mm. The duct of the distributed ducted fan unit is shown in Figure 8. The duct has an inlet length of $l_{in} = 50$ mm, an inlet radius of $R_{in} = 85$ mm, an outlet length of $l_{out} = 100$ mm, a length of the blade section of $l_h = 100$ mm, a radius of the inner wall of $R = 75$ mm, a hub radius of $R_h = 30$ mm, and a maximum radius of the outer wall of $R_{max} = 97.5$ mm.

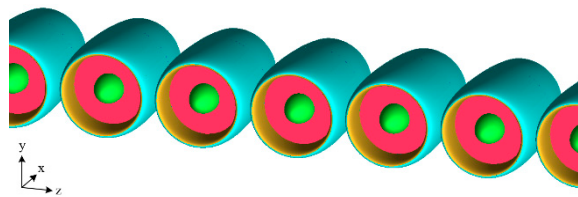


Figure 7. Schematic diagram of the distributed ducted fan system.

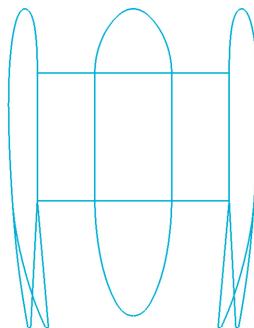


Figure 8. Schematic of the variable area nozzle.

In order to take into account the hover and cruise performance of the distributed ducted fan system, the variable area nozzle (VAN) [24] was adopted as shown in Figure 8. The expanded outlet was used in hover flight to increase the flow velocity of the blade section, and the contracted outlet was adopted in cruise flight to decrease the flow velocity of the blade section, so that the operating point of the rotor and stator in different flight phases was close.

The rotor and stator of the ducted fan were designed in hover flight, using airfoils as shown in Figure 9. The airfoil camber is constant, and the airfoil thickness decreases linearly from the root to the tip. The geometric information of the rotor and stator is shown in Figure 10. The blade number of the rotor is ten, the blade number of the stator is six, and blade tip clearance is 0.5 mm.

It can be seen from Figure 7 that the distributed ducted fan has a high degree of repeatability along the span. In order to improve the efficiency of the calculation and design, a ducted fan unit is selected and its two sides are set as symmetrical boundaries, as shown in Figure 11. The MRF method was used to analyze the characteristics of the distributed ducted fan system.

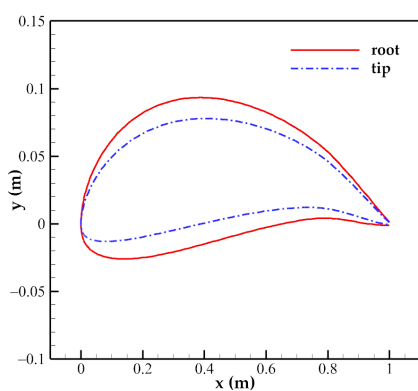


Figure 9. Airfoils of the blade of the ducted fan.

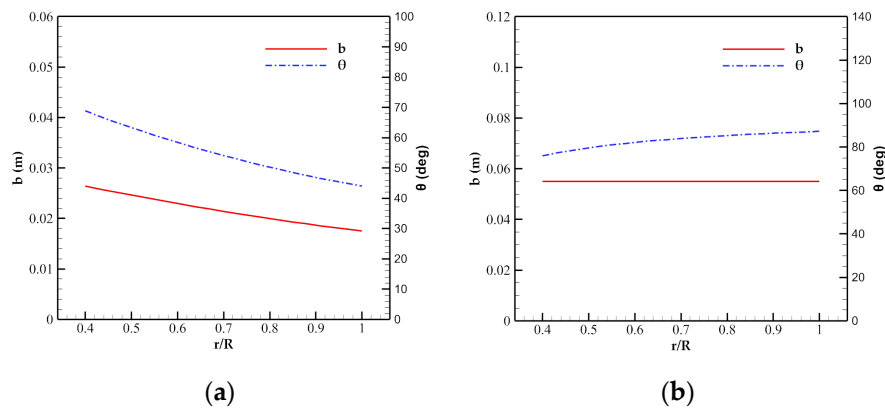


Figure 10. Distribution of the chord length and torsional angle of the rotor and stator: (a) Rotor; (b) Stator.

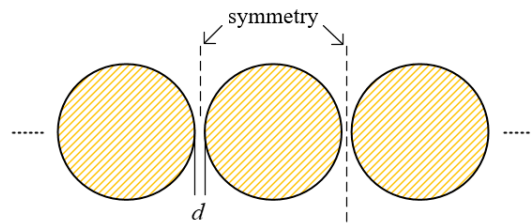


Figure 11. Schematic diagram of the calculation unit of the distributed ducted fan system.

3.2. Performance Analysis

The thrust demand of the distributed ducted fan unit in hover flight is $T = 40$ N, and the hover performance of the distributed ducted fan unit is shown in Table 2, where pl is the power load calculated according to Equation (2). The outlet expansion angle of the ducted fan is $\alpha_e = 3^\circ$.

$$pl = \frac{T}{\Omega Q_r} \quad (2)$$

Table 2. Hover performance of the distributed ducted fan unit.

α_e (deg)	Ω (rpm)	T (N)	T_r (N)	Q_r (N·m)	T_s (N)	Q_s (N·m)	pl (kg·kw ⁻¹)
3	10,850	40.369	16.195	1.061	2.524	1.072	3.349

In cruise flight of $V_0 = 50$ m/s, the thrust demand of the distributed ducted fan unit is $T = 4$ N, and the cruise performance of the distributed ducted fan unit can be improved by adjusting the outlet expansion angle. The efficiency η of the ducted fan is calculated through Equation (3).

$$\eta = \frac{TV_0}{\Omega Q_r} \quad (3)$$

It can be seen from Figure 12 that at $\Omega = 8500$ r/min, the thrust and efficiency of the distributed ducted fan unit are improved with the decrease of outlet expansion angle, and the best outlet expansion angle is $\alpha_e = -5^\circ$. The efficiency of the distributed ducted fan unit under cruise thrust demand is only 35.136%, as shown in Table 3.

Comparing the pressure distribution of the distributed ducted fan unit in two flight phases, as shown in Figures 13 and 14, it can be seen that the mutual influence between the ducted fans reduces the low pressure near the inlet. The low pressure changes little in hover flight, and the flow between the adjacent ducts accelerates in cruise flight, causing the low pressure area on the outer wall of the duct to move backward. In addition, there is

a flow separation at the tail of the duct, as shown in Figure 15, which seriously affects the cruise performance of the distributed ducted fan unit.

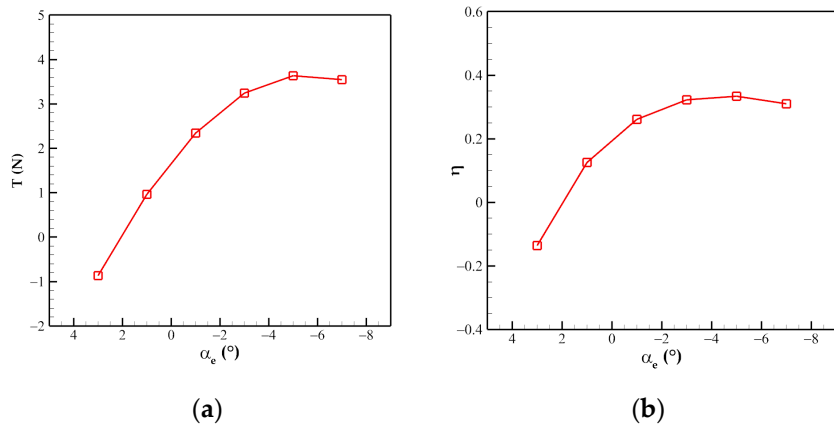


Figure 12. Variation of cruise performance of the distributed ducted fan unit with different outlet expansion angles: (a) Thrust; (b) Efficiency.

Table 3. Cruise performance of the distributed ducted fan unit.

α_e (deg)	Ω (rpm)	T (N)	T_r (N)	Q_r (N·m)	T_s (N)	Q_s (N·m)	η
-5	8610	3.998	8.778	0.631	0.920	0.642	35.136%

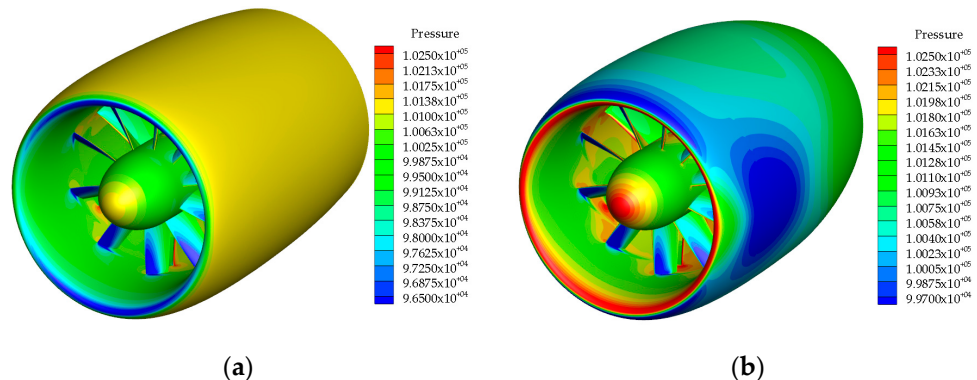


Figure 13. Comparison of surface pressure of the distributed ducted fan unit in different flight phases: (a) Hover; (b) Cruise.

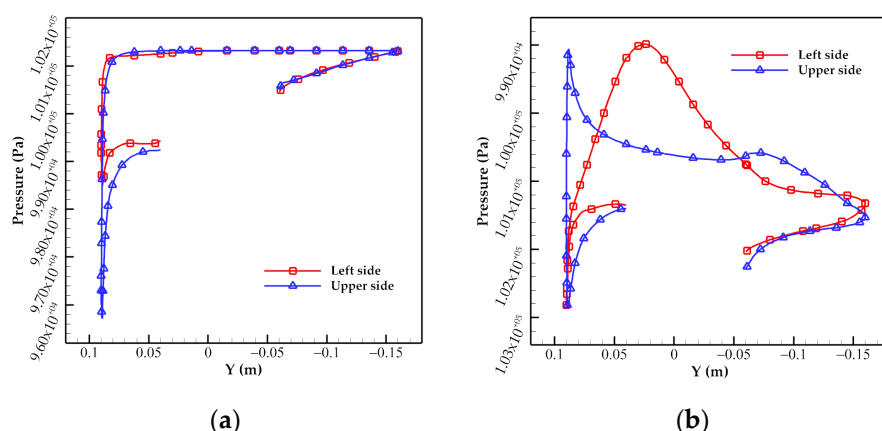


Figure 14. Comparison of the pressure distribution of the duct in different flight phases: (a) Hover; (b) Cruise.

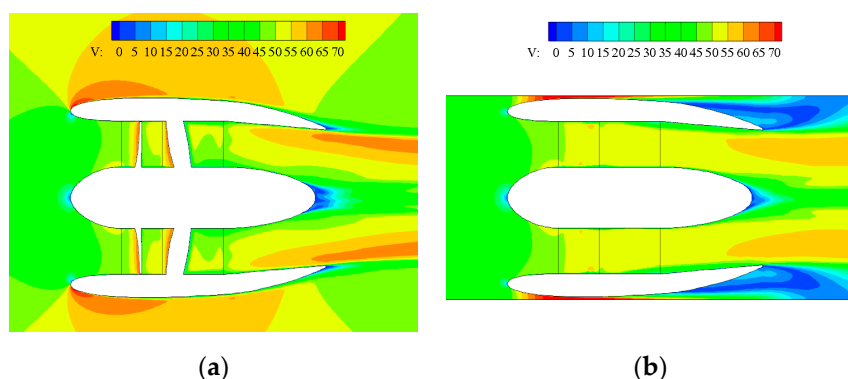


Figure 15. Comparison of the velocity image of the distributed ducted fan unit in cruise flight:
(a) $z = 0$ m; **(b)** $\gamma = 0$ m.

4. New Distributed Ducted Fan System and Related Parameterization Methods

4.1. New Distributed Ducted Fan System

Since the power gap is not conducive to the cruise performance of the distributed ducted fan system, the duct is considered to be rectangular, as shown in Figure 16, to eliminate the power gap.

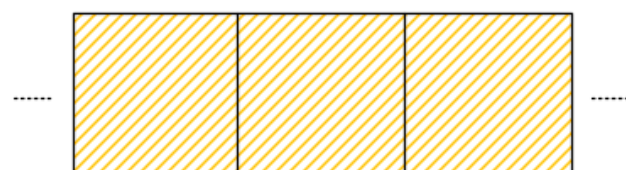


Figure 16. Distributed ducted fan system with the rectangular duct.

In addition, in order to achieve simpler outlet control, the distributed ducted fan system of “ducted fan + induced wing” shown in Figure 17 was adopted. The deflectable induced wing is arranged behind the ducted fan. The symmetrical deflection of the induced wing can realize the expansion and contraction of the wake, and the same direction deflection of the induced wing can be used to generate vertical aerodynamic force.

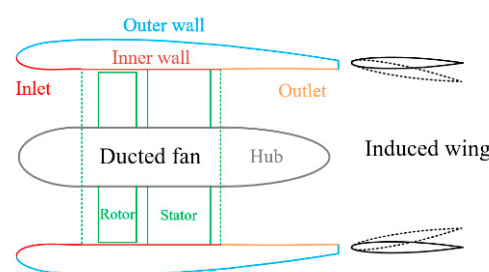


Figure 17. Configuration of the new distributed ducted fan system.

Based on the above analysis, the inlet of the distributed ducted fan unit was designed in the form of "rectangle to circle" and the outlet was designed in the form of "circle to rectangle", as shown in Figure 18. In this way, the ducted fan units of the distributed ducted fan can be seamlessly connected from left to right, and the outer wall of the duct can be shaped like the upper surface of the wing, as shown in Figure 19.

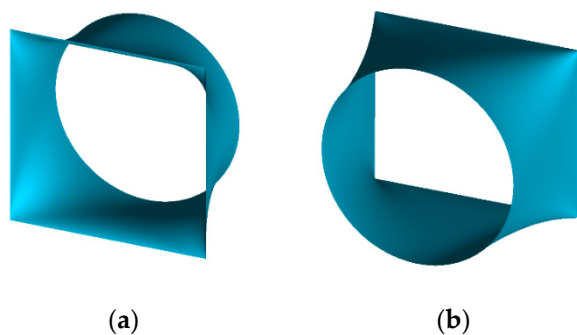


Figure 18. Inlet and outlet of the distributed ducted fan unit: (a) “Rectangle to circle” inlet; (b) “Circle to rectangle” outlet.

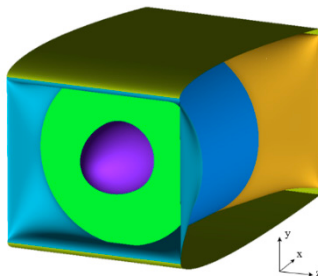


Figure 19. Schematic diagram of the distributed ducted fan unit.

4.2. Parameterization Method of the Inlet and Outlet

4.2.1. Hyperelliptic Equation

The hyperelliptic equation can realize the transition from circle to rectangle, which was widely used in the generation and parameterization of the inlet [22,25]. The hyperelliptic equation is as follows, where a is the major semi-axis, b is the minor semi-axis, and m is the exponent of the hyperelliptic equation.

$$\left(\frac{x}{a}\right)^m + \left(\frac{y}{b}\right)^m = 1 \quad (4)$$

The hyperelliptic equation is an elliptic equation when $m = 2$, and when $m > 2$ and m increases, the hyperellipse is gradually transformed into a rectangle.

4.2.2. Parameterization Method of the Inlet

The inlet of the distributed ducted fan unit adopted the form of “up-down and left-right symmetry”, so only the 1/4 shape of the inlet was parameterized, as shown in Figure 20. The inlet consists of an external inlet and an internal inlet. The internal inlet is a “rectangle to circle” transition surface, and the external inlet is used to connect the internal inlet and the outer wall of the duct. It also can be seen from Figure 20 that the inlet is controlled by three curves: $\mathbf{a}(t)$, $\mathbf{b}(t)$, and $\mathbf{m}(t)$.

The following fourth-order Bezier curves were used to parameterize the three control curves, where $(p_0, p_1, \dots, p_{19})$ are the design variables. The design variables were unitized according to the geometric information, where h_{ii} is the height of the internal inlet, h_{in} is the height of the external inlet, and w_{in} is the inlet width.

$$x(t) = l_{in}[p_0(1-t)^4 + 4p_1t(1-t)^3 + 6p_2t^2(1-t)^2 + 4p_3t^3(1-t) + p_4t^4] \quad (5)$$

$$y_a(t) = R + \left(\frac{w_{in}}{2} - R\right)[p_5(1-t)^4 + 4p_6t(1-t)^3 + 6p_7t^2(1-t)^2 + 4p_8t^3(1-t) + p_9t^4] \quad (6)$$

$$y_b(t) = R + R[p_{10}(1-t)^4 + 4p_{11}t(1-t)^3 + 6p_{12}t^2(1-t)^2 + 4p_{13}t^3(1-t) + p_{14}t^4] \quad (7)$$

$$y_m(t) = R + \left(\sqrt{\left(\frac{w_{in}}{2}\right)^2 + \left(\frac{h_{ii}}{2}\right)^2} - R \right) \cdot [p_{15}(1-t)^4 + 4p_{16}t(1-t)^3 + 6p_{17}t^2(1-t)^2 + 4p_{18}t^3(1-t) + p_{19}t^4] \quad (8)$$

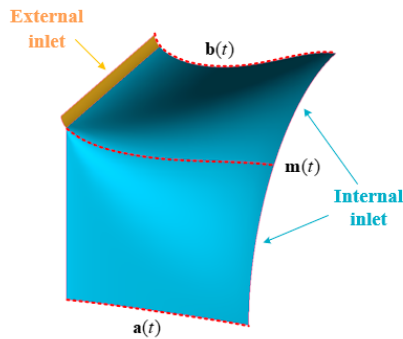


Figure 20. Schematic diagram of the inlet parameterization.

Since the starting point of the Bezier curve is the first control point and the end point is the last control point, the following variables were obtained.

$$p_0 = p_5 = p_{10} = p_{15} = 0 \quad (9)$$

$$p_4 = p_9 = p_{19} = 1 \quad (10)$$

$$p_{14} = (h_{in}/2 - R)/R \quad (11)$$

In order to ensure the horizontal connection between the inlet and the blade section and the vertical connection between the inlet and the outer wall of the duct, the following variables were obtained according to the derivative properties of the Bezier curve.

$$p_6 = p_{11} = p_{16} = 0 \quad (12)$$

$$p_3 = 1 \quad (13)$$

Therefore, there were eight design variables ($p_1, p_2, p_7, p_8, p_{12}, p_{13}, p_{17}, p_{18}$) for the duct inlet.

After determining the three control curves, the information of the major and minor semi-axis of the hyperellipse was obtained directly from the corresponding Bezier curve. The exponent of the hyperelliptic equation was obtained by solving the Equation (14).

$$y_m(t) = \sqrt{(y_b(t) \sqrt[4]{0.5})^2 + (y_a(t) \sqrt[4]{0.5})^2} \quad (14)$$

The length of the internal inlet is l_{ii} , and t_{ii} can be obtained from Equation (15).

$$l_{ii} = x(t_{ii}) \quad (15)$$

When the internal inlet was generated, the variable range of $x(t)$ and $y_b(t)$ was $t \in [0, t_{ii}]$, and the variable range of $y_a(t)$ and $y_m(t)$ was $t \in [0, 1]$. When the external inlet was generated, the variable range of $x(t)$ and $y_b(t)$ was $t \in [t_{ii}, 1]$.

4.2.3. Parameterization Method of the Outlet

The outlet of the distributed ducted fan unit also adopted the form of “up-down and left-right symmetry”, but did not divide the internal and external parts. The outlet design ensured that the end of the upper and lower outlet was horizontal.

Similarly, the fourth-order Bezier curves such as Equations (5)–(8) were used to parameterize the outlet, except that $y_b(t)$ was unitized by Equation (16).

$$y_b(t) = R + \left(\frac{h_{out}}{2} - R\right) [p_{10}(1-t)^4 + 4p_{11}t(1-t)^3 + 6p_{12}t^2(1-t)^2 + 4p_{13}t^3(1-t) + p_{14}t^4] \quad (16)$$

The following variables were obtained according to the characteristics of the outlet and Bezier curve.

$$p_0 = p_5 = p_6 = p_{10} = p_{11} = p_{15} = p_{16} = 0 \quad (17)$$

$$p_4 = p_9 = p_{13} = p_{14} = p_{19} = 1 \quad (18)$$

So, the eight design variables of the duct outlet were ($p_1, p_2, p_3, p_7, p_8, p_{12}, p_{17}, p_{18}$).

When the outlet was generated, the variable range of $x(t), y_a(t), y_b(t)$, and $y_m(t)$ was $t \in [0, 1]$.

5. Multi-Objective Design of the Distributed Ducted Fan System

Multi-objective design was carried out on the ducted fan unit and the corresponding induced wing in the distributed ducted fan system. The specific design steps are shown in Figure 21. Firstly, the multi-objective optimization design of the inlet and outlet of the duct was carried out to obtain the duct geometry. Then, the blade of the distributed duct fan unit was designed in hover flight. Afterwards, the chord length and the deflection angle of the induced wing in cruise flight were designed according to the optimal cruise performance. Finally, the deflection angle of the induced wing was adjusted in the hover flight.

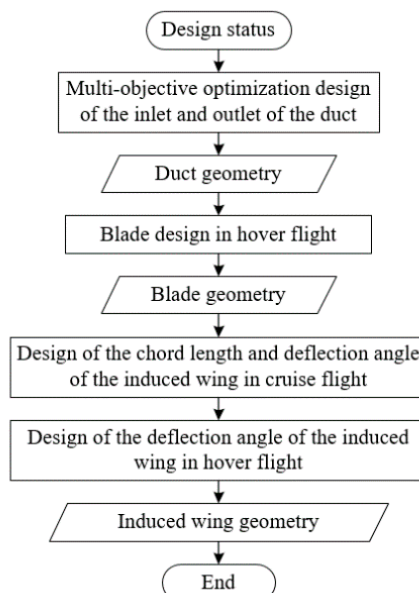


Figure 21. Multi-objective design process of the distributed ducted fan system.

5.1. Multi-Objective Optimization Design of the Inlet and Outlet

5.1.1. Optimization Objectives and Methods

Based on NSGA-II algorithm and Kriging model, the inlet and outlet of the distributed ducted fan unit were optimized. The outer wall of the duct was generated according to the stretching of the NACA0010 airfoil.

Referring to the ducted fan in Section 3.1, the length of the inlet and outlet remained unchanged, the inlet with the width of $w_{in} = 160$ mm and the height of $h_{in} = 140$ mm to keep the inlet area basically consistent, and the outlet with the width of $w_{out} = 160$ mm and the height of $h_{out} = 130$ mm in the basic distributed ducted fan unit.

Then, the effect of increasing the length and height of the inlet was studied. The inlet length was changed to $l_{in} = 70$ mm and $l_{in} = 100$ mm, and the inlet height was changed to $h_{in} = 150$ mm and $h_{in} = 160$ mm. Other geometric parameters remained unchanged.

Since the inlet and outlet adopted the symmetrical form, the optimization was carried out on the 1/4 distributed ducted fan unit. The calculation model is shown in Figure 22, and the left, right, and bottom are set as symmetrical boundary conditions. The grid has 0.44 million cells.

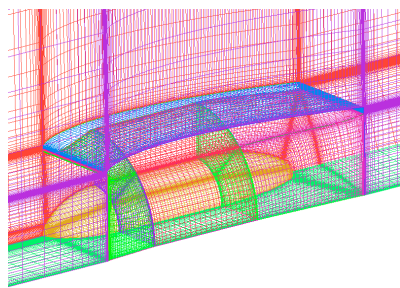


Figure 22. Schematic of the 1/4 calculation model of the multi-objective optimization.

The MSM was used to get the performance of the distributed ducted fan unit. The blade thrust in hover flight is $T_p = 18$ N and in cruise flight is $T_p = 7$ N. Optimization objectives are the maximum duct thrust T_d in hover flight and minimum duct drag D_d in cruise flight.

The initial sample of the Kriging model is 100, and the optimization ends when the sample number exceeds 400. In NSGA-II optimization, the population size is 50, and the maximum evolution number is 1000. The optimization design was carried out in three rounds. Starting from the second round, the Pareto set obtained in the previous round was added to the initial sample in this round to improve the accuracy of the optimization design.

5.1.2. Optimization Results and Analysis

The comparison of different optimization design results is shown in Figures 23 and 24. The results show that the increase of the duct thrust in hover flight contradicts the decrease of the duct drag in cruise flight. The selected design results shown in Figures 23 and 24 were analyzed. “50_80_70” is the result of the basic distributed ducted fan unit, and its three numbers represent the length, width, and height of the 1/4 inlet. The duct thrust is shown in Tables 4 and 5.

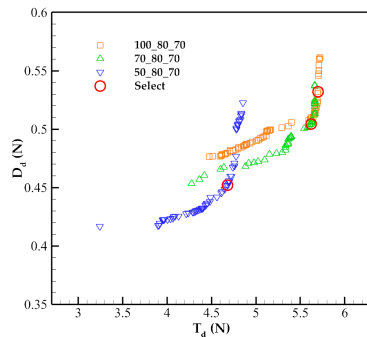


Figure 23. Pareto front of the inlet of different lengths.

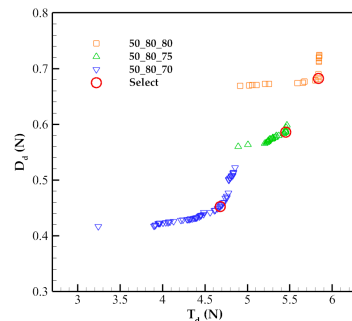


Figure 24. Pareto front of the inlet of different heights.

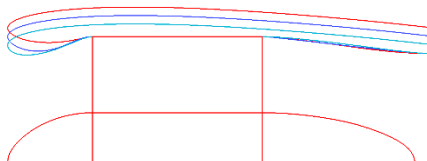
Table 4. Comparison of different optimization results of different inlets in hover flight.

Result	T_d (N)	D_f (N)
100_80_70	5.702	0.258
70_80_70	5.621	0.239
50_80_70	4.683	0.243
50_80_75	5.423	0.241
50_80_80	5.837	0.240

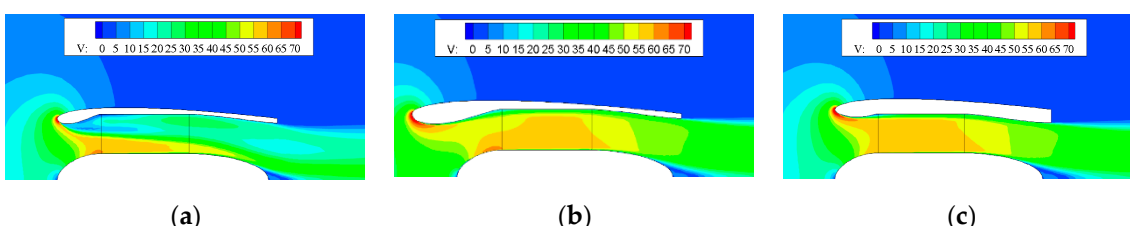
Table 5. Comparison of different optimization results of different inlets in cruise flight.

Result	D_d (N)	D_f (N)
100_80_70	0.532	0.635
70_80_70	0.504	0.597
50_80_70	0.452	0.565
50_80_75	0.586	0.590
50_80_80	0.682	0.613

It can be seen that the difference of the duct in different optimization results is mainly concentrated at the inlet, and the change of the outlet is small, as shown in Figures 25 and 26. The duct thrust of the basic distributed ducted fan unit in hover flight is poor, and increasing the length or height of the inlet is beneficial to improve the duct thrust, but it also increases the cruise drag.

**Figure 25.** Duct profile of the inlet of different lengths.**Figure 26.** Duct profile of the inlet of different heights.

The flow field information is shown in Figures 27–31. In hover flight, there is a strong flow separation at the inlet of the basic ducted fan unit, and the increase in the length and height of the inlet can alleviate the flow separation and increase the duct thrust. However, the increase in the length and height of the inlet expands the windward area and wetted area of the duct, which decreases the duct thrust in cruise flight.

**Figure 27.** Comparison of the velocity image of different optimization results of different inlets in hover flight: (a) 50_80_70; (b) 100_80_70; (c) 50_80_80.

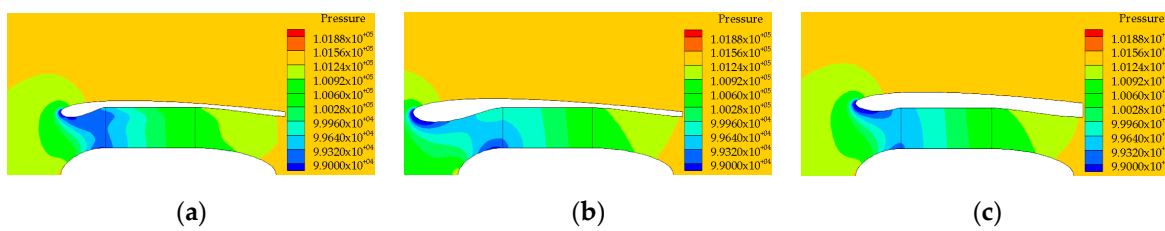


Figure 28. Comparison of the pressure image of different optimization results of different inlets in hover flight: (a) 50_80_70; (b) 100_80_70; (c) 50_80_80.

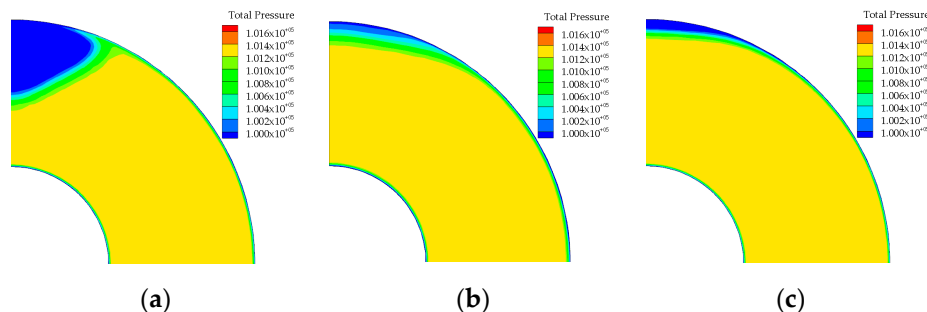


Figure 29. Comparison of the total pressure image at the entrance of the blade section of different inlets in hover flight: (a) 50_80_70; (b) 100_80_70; (c) 50_80_80.

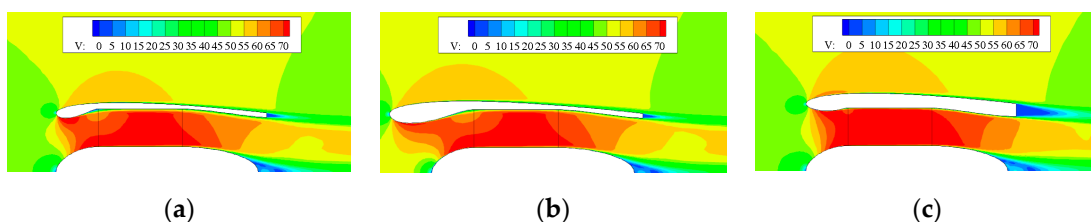


Figure 30. Comparison of the velocity image of different optimization results of different inlets in cruise flight: (a) 50_80_70; (b) 100_80_70; (c) 50_80_80.

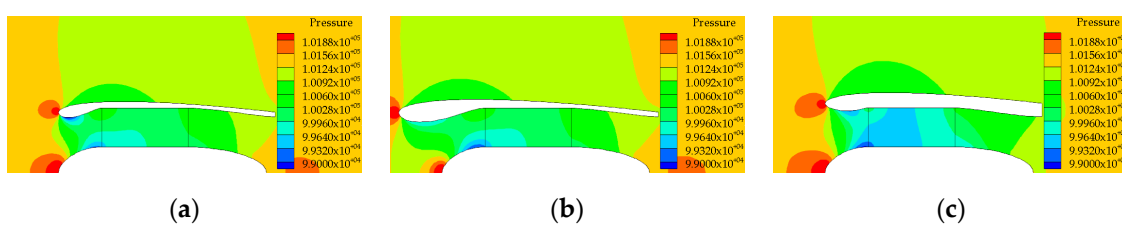


Figure 31. Comparison of the pressure image of different optimization results of different inlets in cruise flight: (a) 50_80_70; (b) 100_80_70; (c) 50_80_80.

The difference of the duct thrust in hover flight between “100_80_70” and “50_80_80” is only 2.368%, but the cruise drag of “50_80_80” increases by 28.195%. In contrast, the increase in inlet height increases the inlet area and has a more significant effect on cruise. In addition, the increase of the inlet area accelerates the flow velocity and reduces the pressure in the blade section in cruise flight, as shown in Figures 31 and 32, which causes the operating point of the rotor and stator in different flight phases far away, adding the difficulty of the multi-objective design.

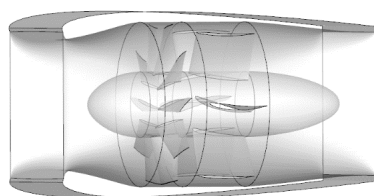


Figure 32. Schematic diagram of the ducted fan unit.

5.2. Blade Design

After obtaining the duct geometry of the distributed ducted fan system, the rotor and stator of the ducted fan were designed in hover flight. In order to compare with the distributed ducted fan system shown in Section 3.1, the same rotor and stator were used without redesign. The ducted fan unit in the distributed ducted fan system is shown in Figure 32.

The hover performance of the ducted fan unit is shown in Table 6. Since the selected design takes into account the cruise performance and is not the best result in hover flight, its power load is reduced by 5.285% compared to the ducted fan unit in Section 3.1.

Table 6. Comparison of the hover performance of the ducted fan unit.

Configuration	Ω (rpm)	T (N)	T_r (N)	Q_r (N·m)	T_s (N)	Q_s (N·m)	pl ($\text{kg}\cdot\text{kw}^{-1}$)
Initial system	10,850	40.369	16.195	1.061	2.524	1.072	3.349
Design	11,000	40.198	17.518	1.100	3.001	1.091	3.172

5.3. Design of the Induced Wing

The main function of the induced wing is to contract the wake of the distributed ducted fan in cruise flight to reduce the flow velocity of the blade section and the inflow angle of the blade element, so that the blade designed in hover flight still has a higher efficiency in cruise flight.

5.3.1. Induced Wing Design in Cruise Flight

The induced wing is 10 mm away from the outlet of the ducted fan and ± 67 mm away from the central axis of the duct, as shown in Figure 33, and adopts the NACA0012 airfoil. Induced wings with chord lengths of 120 mm and 150 mm were used respectively, and the deflection angle (expansion is positive) of the induced wing was changed to evaluate the cruise performance of the distributed ducted fan system.

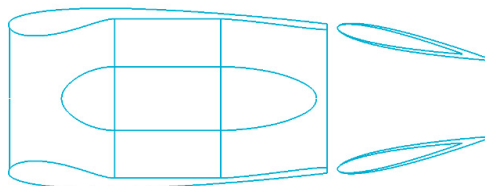


Figure 33. Schematic diagram of the relative position between the ducted fan and induced wing.

The results shown in Figure 34 show that the total thrust and cruise efficiency of the distributed ducted fan system increase with the decrease of the deflection angle of the induced wing. In contrast, the longer induced wing at the same deflection angle makes the wake more fully contracted, and the flow velocity in the blade section is also lower, as shown in Figure 35. The more fully contracted wake makes the rotor and stator closer to the design state, so the cruise performance is better. When the deflection angle continues to increase, the cruise efficiency of the distributed ducted fan system is reduced due to the flow separation occurring on the induced wing. The induced wing with a chord length of 150 mm and a deflection angle of -12° was selected in the cruise flight.

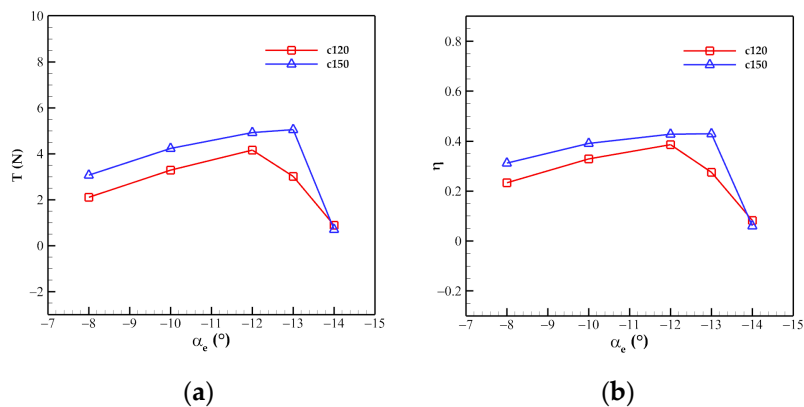


Figure 34. Comparison of the cruise performance of the distributed ducted fan system with different deflection angles of the induced wing at $\Omega = 8500$ r/min: (a) Thrust; (b) Efficiency.

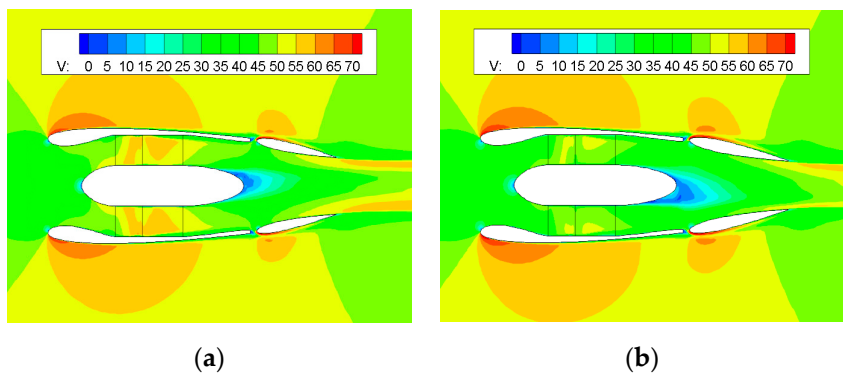


Figure 35. Comparison of sectional velocity image of the distributed ducted fan system with -12° deflection angle of the induced wing with different chord lengths: (a) 120 mm; (b) 150 mm.

The cruise performance of the designed distributed ducted fan system is shown in Table 7. Compared with the distributed ducted fan system in Section 3.1, the cruise efficiency is improved by 11.888%.

Table 7. Cruise performance of the designed distributed ducted fan system.

Configuration	Ω (rpm)	T (N)	T_r (N)	Q_r (N·m)	T_s (N)	Q_s (N·m)	η
Initial system	8610	3.998	8.778	0.631	0.920	0.642	35.136%
Design	8180	3.994	8.662	0.593	1.118	0.601	39.313%

5.3.2. Induced Wing Design in Hover Flight

The influence of the deflection angle of the induced wing on the hover performance of the distributed ducted fan system was analyzed. As shown in Table 8, the performance corresponding to 1° deflection angle is the best. Compared with the ducted fan unit without the induced wing in Table 6, the hovering power load is increased by 1.955%, which is due to the expansion of the wake, as shown in Figure 36. It shows that the induced wing can be used as a contracted outlet to improve the cruise efficiency of the distributed ducted fan system, and can also be used as an expanded outlet to further improve the hover performance of the distributed ducted fan system.

The above design results show that, compared with the distributed ducted fan system in Section 3.1, the unit width of the distributed ducted fan system designed in this paper is reduced from 200 mm to 160 mm, and the spanwise space is reduced by 20%. Although the hovering power load is reduced by 3.434%, the cruise efficiency is improved by 11.888%, which verifies the feasibility of the multi-objective design method of the distributed ducted fan system in this paper.

Table 8. Comparison of the hover performance of the distributed ducted fan system with different deflection angles of the induced wing.

α_e (deg)	Ω (rpm)	T (N)	T_r (N)	Q_r (N·m)	T_s (N)	Q_s (N·m)	pl ($\text{kg}\cdot\text{kw}^{-1}$)
0	11,000	40.068	16.408	1.087	2.425	1.096	3.200
1	11,000	40.347	16.288	1.083	2.392	1.097	3.234
2	11,000	39.623	16.201	1.082	2.343	1.096	3.179

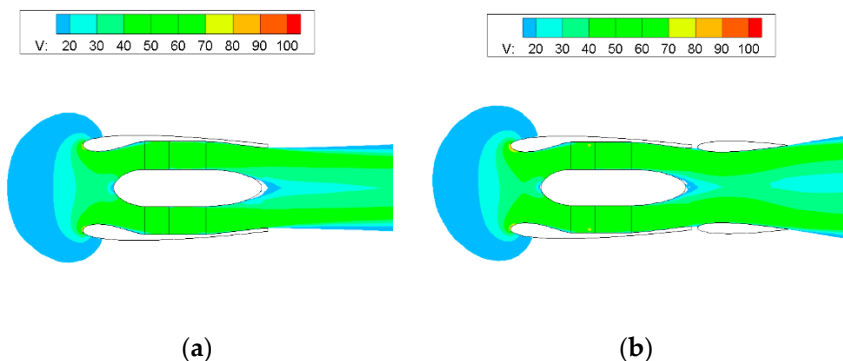


Figure 36. Comparison of the wake of the distributed ducted fan system with and without the induced wing in hover flight: (a) Without the induced wing; (b) With the induced wing.

6. Improved Distributed Ducted Fan System

6.1. Improvement Method

In order to make the wake continue to contract without the flow separation on the induced wing, the height of the duct outlet can be reduced to make a contracted wake before the deflection of the induced wing. At this time, the induced wing with a smaller chord length can be used to reduce the friction drag and improve the cruise performance.

The height of the duct outlet was reduced to $h_{out} = 120$ mm, and the duct inlet remained unchanged. The duct profile of the improved distributed ducted fan system is shown in Figure 37. The induced wing with 120 mm chord length was adopted, and the height of the induced wing from the central axis of the duct was changed to ± 60 mm.

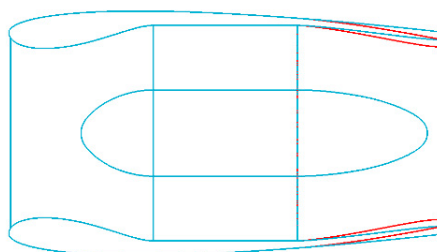


Figure 37. Comparison of duct profile of the distributed duct fan system before and after the improvement.

6.2. Improvement Results

The effect of different deflection angles of the induced wing in cruise flight is shown in Figure 38. The best cruise deflection angle is -12° . The thrust and efficiency of the distributed ducted fan system are better than those before the improvement, which verifies the effectiveness of the improvement method. In hover flight, the power load is the highest when the deflection angle of the induced wing is 2° , as shown in Table 9, indicating that the induced wing makes up for the loss caused by the reduction of the outlet area.

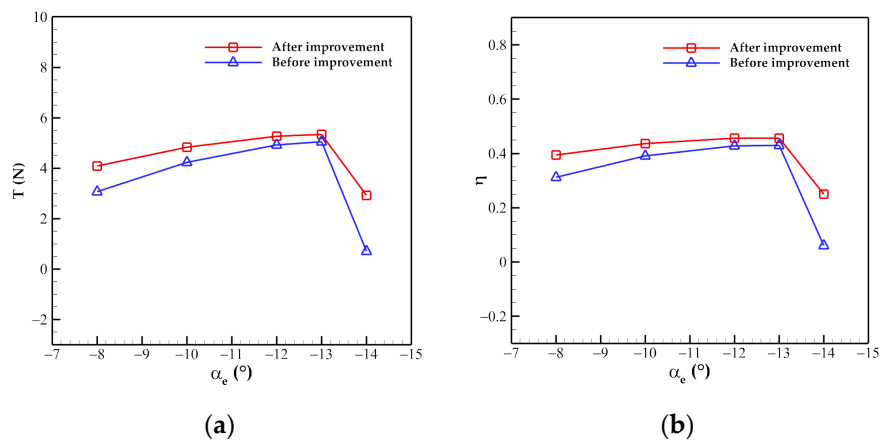


Figure 38. Comparison of the cruise performance of the distributed ducted fan system with different deflection angles of the induced wing before and after the improvement at $\Omega = 8500$ r/min: (a) Thrust; (b) Efficiency.

Table 9. Comparison of the hover performance of the distributed ducted fan system with different deflection angles of the induced wing after the improvement.

α_e (deg)	Ω (rpm)	T (N)	T_r (N)	Q_r (N·m)	T_s (N)	Q_s (N·m)	pl ($\text{kg}\cdot\text{kw}^{-1}$)
0	11,000	40.422	16.775	1.093	2.582	1.097	3.211
1	11,000	40.447	16.589	1.090	2.497	1.097	3.221
2	11,000	40.420	16.482	1.088	2.432	1.096	3.225
3	11,000	40.267	16.419	1.087	2.410	1.095	3.216

In the improved distributed ducted fan system, the chord length of the induced wing is 120 mm, and the deflection angle is 2° in hover flight and -12° in cruise flight, as shown in Figure 39. The induced wing can further expand the wake in hover flight and contract the wake with no flow separation in cruise flight.

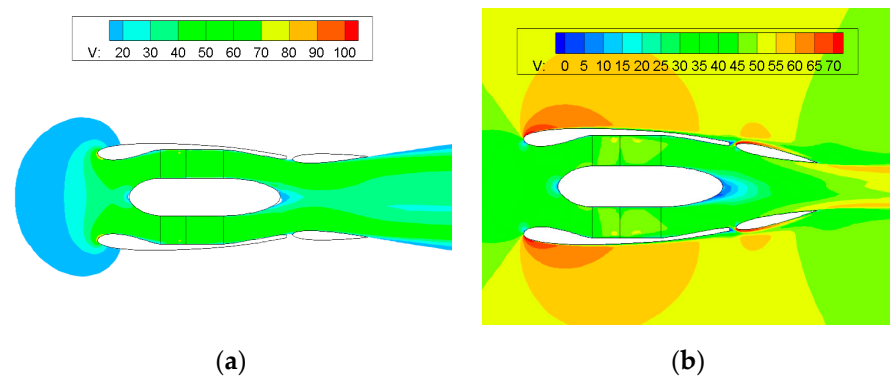


Figure 39. Sectional velocity image of the improved distributed ducted fan system in two flight phases: (a) Hover; (b) Cruise.

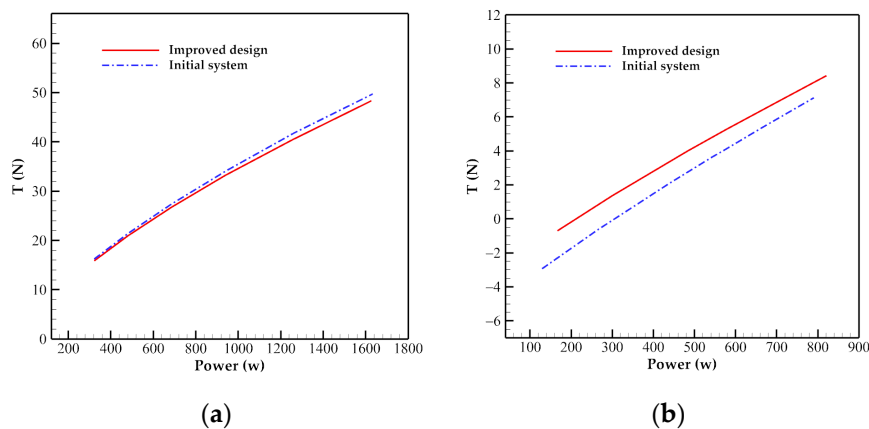
Tables 10 and 11 show the performance comparison of different distributed ducted fan systems under the thrust demand in hover and cruise flight. The improved design improves the cruise efficiency by 4.902% under the condition that the hovering power load remains basically unchanged. Compared with the distributed ducted fan system in Section 3.1, the hovering power load of the improved design is only reduced by 3.703%, but the cruise efficiency is further increased by 17.372%. The performance of the improved distributed ducted fan system is shown in Figure 40.

Table 10. Comparison of the hover performance of different distributed ducted fan systems.

Configuration	Ω (rpm)	T (N)	T_r (N)	Q_r (N·m)	T_s (N)	Q_s (N·m)	pl ($\text{kg} \cdot \text{kW}^{-1}$)
Initial system	10,850	40.369	16.195	1.061	2.524	1.072	3.349
Design	11,000	40.347	16.288	1.083	2.392	1.097	3.234
Improved design	11,000	40.420	16.482	1.088	2.432	1.096	3.225

Table 11. Comparison of the cruise performance of different distributed ducted fan systems.

Configuration	Ω (rpm)	T (N)	T_r (N)	Q_r (N·m)	T_s (N)	Q_s (N·m)	η
Initial system	8610	3.998	8.778	0.631	0.920	0.642	35.136%
Design	8180	3.994	8.662	0.593	1.118	0.601	39.313%
Improved design	8050	3.991	8.399	0.574	1.085	0.580	41.240%

**Figure 40.** Hover and cruise performance of the improved distributed ducted fan system: (a) Hover; (b) Cruise.

7. Conclusions

In this paper, a distributed ducted fan system for the VTOL aircraft was proposed, which eliminates the influence of the power gap in design, and the contraction and expansion of the wake were more simply realized by arranging the deflectable induced wing behind the ducted fan. Then, the parameterization method of the inlet and outlet of the distributed ducted fan unit was established, and the multi-objective design method of the distributed ducted fan system was proposed. Finally, the feasibility of the design method was verified by the design and improvement of the distributed ducted fan system. The conclusions are as follows.

1. The power gap of the distributed ducted fan weakens the low pressure near the inlet and has an adverse effect on the distributed ducted fan system, especially in cruise flight, due to the flow separation at the tail of the duct;
2. In the multi-objective design of the inlet and outlet of the distributed ducted fan system, the outlet obtained by the design is basically the same, and the performance change mainly comes from the change of the inlet. By increasing the length and height of the inlet, the flow separation at the inlet is alleviated, and the duct thrust in hover flight is increased, but it increases the cruise drag at the same time. Compared with the increase of the inlet length, the increase of the inlet height on the one hand brings greater cruise drag, and on the other hand increases the flow velocity in the blade section, which makes the multi-objective design of the distributed ducted fan system more difficult;
3. The performance of distributed ducted fan system can be improved by expanding the wake in hover flight and contracting the wake in cruise flight by the induced wing. The design results show that compared with the distributed ducted fan system composed of the traditional circular ducted fan, the hovering power load of the distributed ducted fan system of the final design is only reduced by 3.703%, but the cruise efficiency is increased by 17.372%, and the spanwise space is reduced by 20%.

Future research will establish a full geometric parameterization model of the ducted fan and induced wing for an integrated design, and further develop the multi-objective optimization design of the overwing distributed ducted fan system.

Author Contributions: Conceptualization, Z.Z. and J.G.; Methodology, J.G.; Software, J.G.; Validation, J.G.; Formal analysis, J.G.; Investigation, J.G. and Z.Z.; Resources, Z.Z.; Data curation, J.G.; Writing—original draft preparation, J.G.; Writing—review and editing, J.G. and Z.Z.; Visualization, J.G.; Supervision, Z.Z.; Project administration, Z.Z.; Funding acquisition, Z.Z. All authors have read and agreed to the published version of the manuscript.

Funding: This research was funded by the Civil Aircraft Specific Project of China (MJ-2015-F-009), Shaanxi Provincial Key Research and Development Program (2021ZDLGY09-08), and Natural Science Basis Research Plan in Shaanxi Province of China (2022JQ-060).

Institutional Review Board Statement: Not applicable.

Informed Consent Statement: Not applicable.

Data Availability Statement: Not applicable.

Conflicts of Interest: The authors declare no conflict of interest.

References

- Smith, A.; Roberts, H.E. The jet airplane utilizing boundary layer air for propulsion. *J. Aeronaut. Sci.* **1947**, *14*, 97–109. [CrossRef]
- Ko, A.; Schetz, J.A.; Mason, W.H. Assessment of the Potential Advantages of Distributed-Propulsion for Aircraft. ISABE 2003–1094. 2003. Available online: https://www.researchgate.net/publication/238191818_Assessment_of_the_Potential_Advantages_of_Distributed_Propulsion_for_Aircraft (accessed on 1 February 2022).
- Stoll, A.M.; Bevirt, J.B.; Moore, M.D.; Fredericks, W.J.; Borer, N.K. Drag Reduction through Distributed Electric Propulsion. In Proceedings of the 14th AIAA Aviation Technology, Integration, and Operations Conference, Atlanta, GA, USA, 16–20 June 2014. [CrossRef]
- Gohardani, A.S.; Doulgeris, G.; Singh, R. Challenges of future aircraft propulsion: A review of distributed propulsion technology and its potential application for the all electric commercial aircraft. *Prog. Aerosp. Sci.* **2011**, *47*, 369–391. [CrossRef]
- Kim, H.D.; Perry, A.T.; Ansell, P.J. A Review of Distributed Electric Propulsion Concepts for Air Vehicle Technology. In Proceedings of the 2018 AIAA/IEEE Electric Aircraft Technologies Symposium, Cincinnati, OH, USA, 9–11 July 2018. [CrossRef]
- Lundbladh, A. Distributed Propulsion and Turbofan Scale Effects. ISABE 2005-1122. 2005. Available online: https://publications.lib.chalmers.se/records/fulltext/10074/local_10074.pdf (accessed on 1 February 2022).
- Alrashed, M.; Nikolaidis, T.; Pilidis, P.; Jafari, S. Utilisation of turboelectric distribution propulsion in commercial aviation: A review on NASA’s TeDP concept. *Chin. J. Aeronaut.* **2021**, *34*, 48–65. [CrossRef]
- Felder, J.L.; Tong, M.T.; Chu, J. Sensitivity of Mission Energy Consumption to Turboelectric Distributed Propulsion Design Assumptions on the N3-X Hybrid Wing Body Aircraft. In Proceedings of the 48th AIAA/ASME/SAE/ASEE Joint Propulsion Conference & Exhibit, Atlanta, GA, USA, 30 July–1 August 2012. [CrossRef]
- Wick, A.T.; Hooker, J.R.; Hardin, C.J.; Zeune, C.H. Integrated Aerodynamic Benefits of Distributed Propulsion. In Proceedings of the 53rd AIAA Aerospace Sciences Meeting, Kissimmee, FL, USA, 5–9 January 2015. [CrossRef]
- Kerho, M.F. Aero-Propulsive Coupling of an Embedded, Distributed Propulsion System. In Proceedings of the 33rd AIAA Applied Aerodynamics Conference, Dallas, TX, USA, 22–26 June 2015. [CrossRef]
- Zhang, Y.; Zhou, Z.; Wang, K.; Fan, Z. Influences of distributed propulsion system parameters on aerodynamic characteristics of a BLI-BWB UAV. *J. Northwest. Polytech. Univ.* **2021**, *39*, 17–26. [CrossRef]
- Black, D.; Rohrbach, C. Shrouded Propellers—A Comprehensive Performance Study. In Proceedings of the 5th Annual Meeting and Technical Display, Philadelphia, PA, USA, 21–24 October 1968. [CrossRef]
- Stubblefield, J.M. Numerically-Based Ducted Propeller Design Using Vortex Lattice Lifting Line Theory. Master Thesis, Mechanical Engineering Department, Massachusetts Institute of Technology, Cambridge, MA, USA, 2008.
- Guo, J.; Zhou, Z.; Li, X. An efficient design method for the blade of ducted propeller. *Acta Aeronaut. Astronaut. Sin.* **2021**, *in press*. Available online: <https://hxzb.buaa.edu.cn/CN/10.7527/S1000-6893.2021.25253> (accessed on 1 February 2022).
- Yu, L.; Drukenbrod, M.; Greve, M.; Abdel-maksoud, M. Research on automatic optimization of ducted propeller design based on CFD techniques. *Chin. J. Hydraul.* **2013**, *28*, 438–444. [CrossRef]
- Ye, K.; Ye, Z.; Qu, Z. Aerodynamic optimization method for duct design. *J. Aerosp. Power* **2013**, *28*, 1828–1835. [CrossRef]
- Ji, L.; Li, J.; Fang, Y. The aerodynamic characteristics and parameter optimization design of ducted fan. *Sci. Technol. Eng.* **2019**, *19*, 245–251.
- Perry, A.T.; Ansell, P.J.; Kerho, M.F. Aero-propulsive and propulsor cross-coupling effects on a distributed propulsion system. *J. Aircr.* **2018**, *55*, 2414–2426. [CrossRef]

19. Yu, D.; Ansell, P.J.; Hristov, G. Aero-Propulsive Integration Effects of an Overwing Distributed Electric Propulsion System. In Proceedings of the AIAA Scitech 2021 Forum, Virtual Event, 11–15 and 19–21 January 2021. [[CrossRef](#)]
20. Bento, H.F.; Vries, R.D.; Veldhuis, L.L. Aerodynamic Performance and Interaction Effects of Circular and Square Ducted Propellers. In Proceedings of the AIAA Scitech 2020 Forum, Orlando, FL, USA, 6–10 January 2020. [[CrossRef](#)]
21. Sun, P.; Zhou, Z.; Guo, J. Numerical analysis for propulsion characteristics of ducted fans in different shapes. *J. Aerosp. Power*, 2021, *in press*. [[CrossRef](#)]
22. Wang, H.; Wang, Y.; Zhou, F.; Liu, H. Optimization design of inlet for distributed ducted fan propulsion system based on panel method. *J. Propuls. Technol.* **2021**, *42*, 2465–2473.
23. Rajagopalan, R.; Zhang, Z. Performance and Flow Field of a Ducted Propeller. In Proceedings of the 25th Joint Propulsion Conference, Monterey, CA, USA, 12–16 July 1989. [[CrossRef](#)]
24. Hall, C.A.; Crichton, D. Engine Design Studies for a Silent Aircraft. *J. Turbomach.* **2007**, *129*, 1653–1662. [[CrossRef](#)]
25. Liu, L.; Song, Y.; Chen, H.; Chen, F.; Cui, K. Design and optimization of half flush-mounted s-shaped inlet. *J. Propuls. Technol.* **2014**, *35*, 1303–1309. [[CrossRef](#)]